

Brownian Dynamics Studies on DNA Gel Electrophoresis. II.

‘Defect’ Dynamics in the Elongation-Contraction Motion

Ryuzo Azuma

Institute for Solid State Physics, The university of Tokyo

*5-1-5 Kashiwanoha, Kashiwa, Chiba 277-8581, Japan**

(Dated: November 21, 2018)

Abstract

By means of the Brownian dynamics (BD) method of simulations we have developed, we study dynamics of individual DNA undergoing constant field gel electrophoresis (CFGE), focusing on the relevance of the ‘defect’ concept due to de Gennes in CFGE. The corresponding embodiment, which we call *slack beads* (s-beads) is explicitly introduced in our BD model. In equilibrium under a vanishing field the distance between s-beads and their hopping range are found to be randomly distributed following a Poisson distribution. In the strong field range, where a chain undergoes the elongation-contraction motion, s-beads are observed to be alternatively annihilated in elongation and created in contraction of the chain. On the other hand, the distribution of hopping range of s-beads does not differ much from that in equilibrium. The results indicate that the motion of the chain elongated consists of a huge number of random movements of s-beads. We have also confirmed that these features of s-beads agree qualitatively with those of s-monomers in the extended bond fluctuation model (EBFM) which we recently proposed. The coincidence of the two simulations strongly supports the stochastic semi-local movement of s-monomers which we *a priori* introduced into the EBFM.

I. INTRODUCTION

Gel electrophoresis is a major technique which separates polyelectrolytes according to their size. Among them gel electrophoresis of DNA is one of the most interesting problems of statistical physics of polymers. Computer simulations^{1,2} and experiments^{3,4} reported a peculiar behavior of individual DNA that they exhibit contracted and extended forms alternatively under a constant field. Recently we have developed a Brownian dynamics (BD) method which simulates electrophoresis of DNA in a 3 dimensional (3D) space by a chain of electrolyte beads. Its details have been reported in our preceding paper (hereafter referred to as I), where we have demonstrated ‘quasi-periodic’ time evolution of the velocity of the center of mass, $v_G(t)$, and of the radius of the longer principal axis, $R_l(t)$, of the chain. The present paper is devoted to clarify the role of ‘defects’ introduced by de Gennes⁵ on the elongation-contraction motion.

The concept of ‘defect’ proposed by de Gennes⁵ is useful to investigate dynamics of individual polymers confined to a space with entanglement such as gel electrophoresis of DNA. A defect represents a relatively loose portion, or a slack segment, of a polymer and is assumed to behave as a particle of ideal gas. He showed that its diffusion in the tube made of other polymers leads to the famous growth law $\phi(t) \propto t^{1/4}$ in the short time regime, where $\phi(t)$ is the mean square displacement of a segment in equilibrium.

Electrophoresis of a chain in an ideal regular network of other fixed chains has been extensively studied by Monte Carlo (MC) simulations.^{6,7,8} Among them, the repton model proposed by Rubinstein is important.⁹ It simulates dynamics of a chain only by stochastic movements of reptons each of which can be regarded as embodiment of a defect. The model is applied to simulation of the constant field gel electrophoresis (CFGE) by Duke.⁷ It was shown that the mobility is inversely proportional to the number of reptons in a very weak field region. The relation was consistent with what the reptation theory predicted under the vanishing field limit.^{10,11} Under finite fields, however, the results derived from the repton model qualitatively differ from those derived from the biased reptation theory¹²: the mobility plateau is reached at lower fields in the former model than those predicted by the latter theory. Duke also observed snapshots of tubes which look like hooks, and argued that once a chain is hooked around a gel fiber, both its arms tend to stretch and rarely retract. This is because defects prefer to move in direction of the field and to create new

tube segments which in turn prefer to align to the field. The observed fact that the chain rarely exhibits a retraction is considered to be an artifact of the MC method which uses local hopping rules. The incorporation of a hopping rule which allows non-local movement of defects was done by Duke and Viovy in their advanced version of the repton model.^{13,14} Simulations of chains with over a thousand segments revealed that a chain exhibits ramified configurations where ‘hernias’ are created and annihilated under a constant field.¹³

Recently, we have investigated gel electrophoresis and diffusive dynamics of a chain in a space with immobile obstacles by making use of an extended version of the bond fluctuation model (BFM).¹⁵ The conventional BFM (CBFM)¹⁶ is known as an efficient model to simulate general problems involved in polymers. However, it is faced with a problem which is similar to that of the repton model mentioned above: the chain motion extremely slows down when it is applied to CFGE under relatively large fields.⁸ To overcome this problem, we have empirically incorporated semi-local dynamics of slack parts of a chain. The latter correspond to ‘defects’ due to de Gennes and were named s-monomers. They are explicitly defined in each configuration appearing in the CBFM. We have called such a BFM with introduction of semi-local movements of s-monomers the extended BFM (EBFM). Both the DV model and the EBFM incorporate nonlocal movements of slack portions of DNA. There are, however, the following difference between the two methods. In the DV model any defect is not created or annihilated except at the extremity, whereas in the EBFM, s-monomers are continually created and annihilated anywhere in the chain, since it involves the CBFM trials of conventional local movements of all monomers.

Using the EBFM it has been confirmed that the trapping problem of the CBFM under large fields is overcome and the field-dependence of mobility is reproduced qualitatively as observed by the experiment.¹⁷ Furthermore, quasi-periodic behavior, or a damped oscillation, is observed in the correlation function of $R_l(t)$ in 3D¹⁸ as it has been observed in the experiment^{3,4} as well as by the BD calculations in 2D (without the excluded volume effect)¹⁹ and in 3D (with the effect).²⁰

The defect is thus a quite important concept to understand DNA dynamics in gel. The purpose of the present paper is to clarify the microscopic bases of the defect dynamics, thereby presenting a microscopic support of the EBFM. For this purpose we examine the corresponding object in a chain, i.e., slack beads (abbreviated as s-beads) by means of the BD method. The work which is similar to this approach has been done by Masubuchi et al.²¹

in their 2D BD study on the biased sinusoidal field gel electrophoresis (BSFGE). Looking at time evolution of snapshots of kinks which correspond to slack segments, they have found that a portion with less kinks develops near the segment which is hindered by an obstacle, and that the portion gradually shifts as the chain slides off the obstacle. They have argued that the growth of kinks plays a key role on the decrease of the mobility observed in chains with particular sizes under BSFGE.

In the present paper we examine static and dynamic properties of defects much more in details by means of our BD method for a chain in a 3D space. As described in our accompanying paper, hereafter referred to as I,²⁰ the method incorporates semi-microscopic ingredients of dynamics of a polymer, i.e., the excluded volume effect, the non-linear elastic force which keeps the distance between the two adjacent beads (segments) and the random force from a solvent. In each configuration of the chain simulated by the BD method s-beads, or ‘defects’, are explicitly specified in a quite similar way as the s-monomers have been defined in the EBFM. Then we investigate various statistics associated with the s-beads, or more explicitly, portions between the neighboring s-beads which we call extended parts of the chain.

In particular, we have concentrated on the normalized histogram of the extended parts of length n , $r_n(t)$, and that of their displacement along the chain direction, $r_{\Delta u}(t)$. In equilibrium under a vanishing field it is found that both $r_n(t)$ and $r_{\Delta u}(t)$ obey Poisson distributions as expected. In the elongation-contraction motion under CFGE, $r_n(t)$ exhibits a peculiar time evolution reflecting the elongation and contraction of the chain. The histogram $r_{\Delta u}(t)$, on the other hand, does not fluctuate correspondingly to $r_n(t)$ but exhibits random hopping nature rather similar to the one observed in equilibrium. These results indicate that defects move quite stochastically even in the *deterministic* regime where the chain elongation-contraction motion looks apparently deterministic. These features of $r_n(t)$ and $r_{\Delta u}(t)$ are confirmed to be in qualitative agreement with those observed for s-monomers in the EBFM.

The organization of the present paper is as follows. In the next section we briefly explain our numerical method, and discuss equilibrium dynamics of s-beads in Sec. III. Characteristic features of $r_n(t)$ and $r_{\Delta u}(t)$ in the field range where a chain exhibits elongation-contraction motions are examined in Sec. IV. The corresponding results obtained by the EBFM are discussed in Sec. V, and the final section is devoted to the conclusion.

II. NUMERICAL METHOD

The BD method we adopt in the present work is to solve the following Langevin equation of motion for a chain of spherical beads in a continuous 3D space,

$$\zeta \dot{\mathbf{x}}_i = q \mathbf{E}_b + \sum_{\alpha} \sum_j \mathbf{S}_{ij}^{\alpha} + \sum_{\alpha} [\mathbf{F}_i^{\alpha} - \mathbf{F}_{i-1}^{\alpha}] + \mathbf{f}_i, \quad (1)$$

where \mathbf{x}_i is the position of the i -th bead, and ζ , q , and \mathbf{E}_b are the viscosity, the charge of a bead and the (bare) external field, respectively. The second and the third terms in r.h.s. are the constraining forces required for the beads to satisfy the conditions,

$$\|\mathbf{x}_{ij}\| = \|\mathbf{x}_j - \mathbf{x}_i\| > 1 \quad (2)$$

$$\|\mathbf{l}_i\| = \|\mathbf{x}_{i+1} - \mathbf{x}_i\| < \sqrt{2}. \quad (3)$$

putting the bead diameter unity. The last term in eqn. 1 stands for the random force from a solvent. Explicitly we adopt the following form for it

$$\mathbf{f}_i(t) = \sum_n \mathbf{f}_i^n \delta(t - n\Delta t), \quad (4)$$

where Δt is regarded as the average period of random forces. The distribution of \mathbf{f}_i^n is characterized by the averages

$$\langle \mathbf{f}_i^n \rangle = \mathbf{0} \quad (5)$$

$$\langle \mathbf{f}_i^m \mathbf{f}_j^n \rangle = 2\zeta k_B T \Delta t \delta_{ij} \delta_{mn}. \quad (6)$$

Here k_B and T are the Boltzmann constant and the absolute temperature, respectively.

The details of solution of the above set of equations have been explained in our accompanying paper I. As a representative of ‘defect’, or a loose portion of a chain in the BD calculation we define a slack bead (s-bead). For any sequences of three beads, if the distance between the first and the third is not greater than $\sqrt{2}$, the second one is regarded as an s-bead. This definition of ‘defect’ is the same as that of s-monomers in a 3D version of the EBFM we investigated before¹⁸ (see in Sec. V). We call a sequence of beads between neighboring s-beads an extended part of the chain.

III. ‘DEFECTS’ IN EQUILIBRIUM

In equilibrium under a vanishing field, ‘defects’ are considered to be distributed randomly along the polymer coordinate. Correspondingly, in our BD analysis, s-beads are randomly

distributed throughout the chain. Then the ‘extended’ parts consisting of n beads is expected to obey a distribution

$$\Psi(n) = \frac{(M-n)(1-\rho)^n}{\sum_{i=1}^M (M-i)(1-\rho)^i}, \quad (7)$$

where M is the total number of beads of the chain and ρ the density of s-beads. For $M \gg n \gg 1$, $\Psi(n)$ reduces to a Poisson distribution:

$$\Psi(n) \cong \rho(1-\rho)^n = \rho e^{-n \log(\frac{1}{1-\rho})}. \quad (8)$$

Next let us consider Δu , displacement of the tangential component, of extended parts between neighboring s-beads. In our BD calculation, it is evaluated as

$$\Delta u \equiv \left| \sum_{i=i_m}^{i_{m+1}} \Delta s_i \right|, \quad \text{with} \quad \Delta s_i = \Delta \mathbf{x}_i \cdot \frac{\mathbf{x}_{i-1} - \mathbf{x}_{i+1}}{\|\mathbf{x}_{i-1} - \mathbf{x}_{i+1}\|} \quad (9)$$

where $\Delta \mathbf{x}_i$ is the displacement of the i -th bead in one MD step solving the Langevin equation 1 and index i_m denotes a figure which is numbered on the s-beads. From eqn. 1 we may assume that the distribution of $\Delta \mathbf{x}_i$ is essentially given by that of the random force, \mathbf{f}_i^n , defined by eqn. 6. Then the distribution of Δs_i is written as

$$\Xi(\Delta s_i) = \sqrt{\frac{\zeta}{2\pi k_B T}} \exp(-\zeta \Delta s_i^2 / 2k_B T). \quad (10)$$

Using this $\Xi(\Delta s_i)$ and $\Psi(n)$ of eqn. 8, we can evaluate the distribution of Δu as

$$\begin{aligned} \Phi(\Delta u) &= \int_0^\infty dn \Psi(n) \prod_{i=1}^n \left[\int_{-\infty}^\infty \Xi(\Delta s_i) d\Delta s_i \right] \delta\left(\sum_{i=1}^n \Delta s_i - \Delta u\right) \\ &= \rho \sqrt{\frac{2\pi^2 \zeta}{k_B T \log \frac{1}{1-\rho}}} \exp \left[-\sqrt{\frac{\log \left(\frac{1}{1-\rho}\right)}{k_B T / 2\zeta}} \Delta u \right]. \end{aligned} \quad (11)$$

Thus $\Phi(\Delta u)$ is expected to obey also a Poisson distribution with the width $\Omega_{\Delta u} = 1/\sqrt{\log(\frac{1}{1-\rho})/(k_B T / 2\zeta)}$. The latter is proportional to $\sqrt{k_B T}$ if the T -dependence of ρ is neglected.

In Fig. 1, we show the normalized histograms r_n and $r_{\Delta u}$ in equilibrium for various T which are obtained by the BD calculation. Here $r_n = N_n / \sum_n N_n$ where N_n is the number that the extended parts of a length n appear in the chain configurations simulated, and $r_{\Delta u}$ is similarly defined. In agreement with $\Psi(n)$ of eqn. 8 r_n obeys a Poisson distribution. The

exponential tail of r_n at $k_B T = 1$ is fitted to $e^{-n/\omega}$ with $\omega \equiv \langle n \rangle \cong 5.7$, which yields $\rho \cong 0.17$ through the relation $\omega = 1/\log\left(\frac{1}{1-\rho}\right)$. In the simulation we have also directly counted the number of s-beads, which yields the same s-bead density $\rho \cong 0.17$ as expected. The distribution $r_{\Delta u}$ of the tangential movement of the extended parts, which we regard as that of the s-beads, also obeys a Poisson distribution as seen in the same figure. Its exponential tail, specified by $\Omega_{\Delta u}$ as $e^{-n/\Omega_{\Delta u}}$, significantly depends on T . As shown in Fig. 2, its dependence on T is consistent with eqn. 11. Even the pre-factor 0.30 of the proportionality to $\sqrt{k_B T}$ agrees with the predicted value $1/\sqrt{2 \log \frac{1}{1-\rho}} \cong 0.37$ within 20%.

The results obtained above confirm the role of the ‘defects’, or the s-beads, on the static and dynamic properties of a polymer in equilibrium. In particular, it is natural to regard $c\langle n \rangle \langle l \rangle$ as the ‘persistence length’ of the chain, where $\langle n \rangle$ is the mean value of n and c is a numerical constant nearly equal to unity. In this context, we note $\sqrt{2} > \langle l \rangle > 1$, where $\langle l \rangle$ is the mean distance between two adjacent beads. In fact we have already argued in I that this interpretation yields an appropriate conversion factor between the length scales of the BD simulation and the experiment. Here we have to emphasize that the value of $\langle n \rangle$ is almost independent of T in the range $k_B T \lesssim 8$, as well as of M and a_{gel} we have examined. It is observed, however, to reduce about by a half when the excluded volume effect between beads is discarded. This enlargement of the ‘persistence length’ is one of the important consequences of the excluded volume effect on the present BD chain in a 3D space.

IV. ‘DEFECTS’ DYNAMICS UNDER CFGE

Under relatively strong fields DNA undergo the quasi-periodic behavior⁴: real time images of individual DNA exhibit elongated and contracted shapes alternatively. Corresponding behavior was observed in the previous 2D BD models^{1,19,22} likewise by our present BD simulation which has been discussed in details in I. We show in Fig. 3, a normalized curve of $R_l(t)$, i.e., $\bar{R}_l(t - t_{\text{max}})/\bar{R}_l(t_{\text{max}})$ of chains with $M = 160$ in a lattice of gel with the lattice distance of $a_{\text{gel}} = 20$ under a field $E \equiv qE_b = 0.032$. In order to get further insights into the mean elongation-contraction motion through the defect dynamics, we have examined histograms of length of the extended parts $N_n(t)$ and of their tangential movement $N_{\Delta u}(t)$ at four representative time intervals, i.e., $[t_{\text{min}} - 0.1D, t_{\text{min}}]$, $[t_{\text{min}}, t_{\text{min}} + 0.1D]$, $[t_{\text{max}} - 0.1D, t_{\text{max}}]$, and $[t_{\text{max}}, t_{\text{max}} + 0.1D]$, as indicated in Fig. 3. Here $t_{\text{min}} \equiv \overline{t_{\text{min}:l}^n} - t_{\text{max}}^n$

and $D \equiv \overline{t_{\min:r}^n - t_{\min:l}^n}$, where t_{\max}^n is the time of local maximum in the n -th peak in $R_l(t)$, $t_{\min:r}^n$ and $t_{\min:l}^n$ are respectively local minima just before and after the local maximum at t_{\max}^n , and the overline stands for the average over peaks in $R_l(t)$. As for the procedure how to pick up the peaks in $R_l(t)$, the reader may refer to I. We denote the four intervals introduced here as Interval 1, 2, 3 and 4, respectively. It is expected that Interval 1 corresponds to the time range where the chain is in a coiled shape, Interval 2 to that of a contracted shape when a U-shape conformation has just started to grow due to trapping by gel, Interval 3 to that of an elongated U-shape when the chain is going to get rid of the trap, and Interval 4 to that of an I-shape when it is going to retrieve another coiled shape. We cut out sequential 2000 MD steps (mds) in each of the four intervals of each peak in $R_l(t)$ and accumulate data associated with them over 80 peaks whose D are about 1.5×10^5 mds or larger.

The normalized histograms $r_n(t)$ ($= N_n(t)/\sum_m N_m(t)$) and $r_{\Delta u}(t)$ thus obtained are shown in Figs. 4 and 5, respectively. They exhibit peculiar time evolution within the ‘elongation-contraction’ period. One may at once notice from $r_n(t)$ that the chain is pulled by the field in Intervals 2 and 3. Particularly in Interval 3, $r_n(t)$ at $40 \lesssim n \lesssim 120$ becomes about 10^{-3} whose integrated weight reaches about 10%, i.e., among 10 extended parts one of them is as large as several tens. The latter is quite elongated and is considered to constitute the longer arm of the U-shaped chain. Interestingly, however, we can see from Fig. 5 that $r_{\Delta u}(t)$ at Δu larger than ten is always negligibly small. This means that sliding dynamics of the chain even in Interval 3 consists of a large number of defect movements whose Δu are less than several times of the mean bead distance. Thus the dynamics even in the elongated portion of the chain is considered to be quite stochastic when it is looked at through Δu , i.e., changes in a unit of time of our BD simulation. In this context, we note here that up to several hundreds multi-scattering processes between beads are involved in one MD step of our BD method as explained in I.

Another interesting observation is that both $r_n(t)$ and $r_{\Delta u}(t)$ in Interval 4 is the most closer, among the four intervals, to a Poisson distribution which is observed in equilibrium under $E = 0$. Namely, although $R_l(t)$ is still relatively larger in this interval just after the chain is released at $t \simeq t_{\max}$ from trapping by an obstacle(s), many s-beads have invaded into the extended part(s) and the chain contracts dominantly by the entropic effect. When $R_l(t)$ comes closer to its local minimum value due to trapping by a new obstacle(s), i.e., in Interval 1, $r_n(t)$ and $r_{\Delta u}(t)$ at larger n and Δu become bigger than those of Interval 4,

indicating that some parts of the chain are already elongated by the field.

Now let us turn to Figs. 6 and 7 where r_n and $r_{\Delta u}$ averaged over the whole time window of the BD run under different fields are shown. Up to the field strength of $E \simeq 0.008$ neither r_n nor $r_{\Delta u}$ significantly deviates from a Poisson distribution, while in r_n under $E \gtrsim 0.016$ a tail clearly shows up at large n . This clearly indicates the existence of a crossover between dynamical regimes with and without the elongation-contraction motion at around $E \simeq 0.008$ with $M = 160$ and $a_{\text{gel}} = 20$. Even in the regime with the elongation-contraction motion where r_n exhibits a significant deviation from a Poisson distribution, Δu remains in an exponential distribution, though its width moderately increases with increasing E . This result again indicates that, even in the *deterministic* regime where the time evolution of averaged $R_l(t)$ or $v_G(t)$ looks apparently deterministic, defect dynamics is still purely stochastic.

V. EXTENDED BOND FLUCTUATION METHOD

The stochastic nature of ‘defect’ dynamics found by the BD method in the present work was just the basic assumption *a priori* introduced in the extended bond fluctuation method (EBFM) when we developed it.¹⁵ The conventional BFM (CBFM)¹⁶ is a well-established MC method which simulate thermodynamic properties of polymers by a coarse-grained chain model on a lattice. It consists of a set of local movements which suffice the conditions necessary for the chain to evolve by self-avoiding random walk. In addition to this local updating process we introduced non-local movements of ‘defects’ in the EBFM. For this purpose ‘defects’, or ‘s-monomers’ are defined in almost the same way as s-beads are defined in the present work. We then let s-monomers hop non-locally within an extended portion of the chain that each s-monomer lies. The movements are incorporated in such a way that they fulfill the detailed valance and the self-avoiding conditions. In the EBFM this non-local movement of s-monomers and the local updating of the CBFM are tried alternatively. We note that the number of s-monomers does not change except at the chain ends by the former process, but it does change anywhere in the chain by the latter updating.

In Fig. 8 we show r_n and $r_{\Delta u}$ of a chain with $M = 80$ obtained in the EBFM under $\Theta = 0$, where we denote the normalized field as $\Theta \equiv qE_b/k_B T$ for the MC analysis. As is the case for the BD model, both r_n and $r_{\Delta u}$ obtained by the EBFM obey a Poisson distribution except

for regions n , $\Delta u \lesssim 5$. Furthermore, in the EBFM, their widths coincide with each other at large n and Δu . In this context, it is noted that we have adopted equal probability of semi-local movement of an s-monomer by any distance k among possible n ones. The width of the distribution r_n of the EBFM is about a half of that of the BD method. Correspondingly, ‘defect’ density ρ ($\simeq 0.33$) of the EBFM is about twice larger than that of the BD method. Although there exist such quantitative differences between the two methods, the qualitative agreement in the results demonstrated in Figs. 1 and 8 supports our EBFM approach in Ref. 15.

The elongation-contraction motion under CFGE is also observed by the EBFM. The normalized histograms $r_n(t)$ and $r_{\Delta u}(t)$ obtained in the four intervals introduced in Sec. IV are shown in Figs. 9 and 10. Their overall features qualitatively agree with those obtained by the BD calculation. By a detailed inspection of Fig. 9, however, we see that $r_n(t)$ in Intervals 2 and 3 by the EBFM still exhibit nearly exponential distributions at larger n in contrast to those of the BD results which have an enhanced tail at n as large as several tens. This difference is considered to originate from the following process of the EBFM: s-monomers are created or annihilated, and so length n of extended parts are changed, only through local updating of monomers originally incorporated by the CBFM. By such local stochastic processes an extremely long extended part is hardly created.

The normalized histogram $r_{\Delta u}(t)$ shown in Fig. 10, on the other hand, exhibit exponential behavior at $\Delta u \gtrsim 2$ quite similar to the corresponding BD result shown in Fig. 5. This is also the case for the integrated distributions $r_{\Delta u}$ under various field strengths. They are shown in Fig. 11 which one can compare with the corresponding BD result in Fig. 7. Quantitatively, $r_{\Delta u}(t)$ and $r_{\Delta u}$ by the EBFM have significant weight at relatively larger Δu as compared with those by the BD calculation. This difference is attributed to the process in the EBFM that, once a long extended part of length n is created, a tangential move of the s-monomer by the distance n is accepted by the probability proportional to $1/n$. Although there exist such minor differences between the dynamical processes involved in the EBFM and the BD method, the results demonstrated above are sufficient for us to conclude that the EBFM properly takes into account the stochastic dynamics of slack segments which give rise to the elongation-contraction motion of a polymer under gel electrophoresis.

VI. CONCLUSION

In equilibrium under a vanishing field it is found, as expected, that s-beads, or ‘defects’, are distributed randomly. Both distributions of extended parts $r_n(t)$ and of their tangential movements $r_{\Delta u}(t)$ obey a Poisson distribution. In the relatively strong field region where a chain exhibits the elongation-contraction motions giving rise to quasi-periodic behavior in $R_l(t)$ and $v_G(t)$, $r_n(t)$ is observed to show the corresponding time evolution. Especially, immediately before $R_l(t)$ reaches to a local maximum, chain conformations with extended parts of more than a few tens of beads, which are entropically unfavorable, are observed. As for $r_{\Delta u}(t)$, such a large fluctuation seems not to occur. We therefore conclude that the s-bead dynamics at a semi-microscopic level is rather stochastic, though the coarse-grained quantities such as $R_l(t)$ look apparently deterministic during the elongation-contraction motion, or in time ranges which we have called *deterministic* ones. We have also shown that these features of $r_n(t)$, $r_{\Delta u}(t)$ and $R_l(t)$ are similar to those observed by the MC analysis based on the EBFM which we recently proposed. Such coincidences between the two simulations strongly support our algorithm of EBFM which requires an order of magnitude less CPU times than MD calculations based on the present BD method do.

Acknowledgments

The author wish to thank H. Takayama for useful discussions and suggestions. The computation in the present work has been done using the facilities of the Supercomputer Center, Institute for Solid State Physics, University of Tokyo, and those of the Computer Center of University of Tokyo.

References

- * Present address: Genomic Sciences Center, RIKEN, 1-7-22 Suehiro, Tsurumi, Yokohama, Kanagawa, 230-0045, Japan
- ¹ J. M. Deutsch, *Science* **240**, 922 (1988).
 - ² J. M. Deutsch and T. L. Madden, *J. Chem. Phys.* **90**(4), 2476 (1989).
 - ³ Y. Masubuchi, H. Oana, K. Ono, M. Matsumoto, M. Doi, K. Minagawa, Y. Matsuzawa, and K. Yoshikawa, *Macromolecules* **26**, 5269 (1993).
 - ⁴ H. Oana, Y. Masubuchi, M. Matsumoto, M. Doi, Y. Matsuzawa, and K. Yoshikawa, *Macromolecules* **27**(21), 6061 (1994).
 - ⁵ P. G. de Gennes, *J. Chem. Phys.* **55**(2), 572 (1971).
 - ⁶ M. O. de Cruz, J. M. Deutsch, and S. F. Edwards, *Phys. Rev. A* **33**(3), 2047 (1986).
 - ⁷ T. A. J. Duke, *J. Chem. Phys.* **93**(12), 9049 (1990).
 - ⁸ J. Batoulis, N. Pistor, K. Kremer, and H. L. Frisch, *Electrophoresis* **10**, 442 (1989).
 - ⁹ M. Rubinstein, *Phys. Rev. Lett.* **59**(17), 1946 (1987).
 - ¹⁰ L. S. Lerman and H. L. Frisch, *Biopolymers* **21**, 995 (1982).
 - ¹¹ O. J. Lumpkin and B. H. Zimm, *Biopolymers* **21**, 2315 (1982).
 - ¹² O. J. Lumpkin, P. Déjardin, and B. H. Zimm, *Biopolymers* **24**, 1573 (1985).
 - ¹³ T. A. J. Duke and J. L. Viovy, *Phys. Rev. Lett.* **68**(4), 452 (1992).
 - ¹⁴ T. A. J. Duke and J. L. Viovy, *J. Chem. Phys.* **96**(11), 8552 (1992).
 - ¹⁵ R. Azuma and H. Takayama, *Phys. Rev. E* **59**(1-B), 650 (1999).
 - ¹⁶ I. Carmesin and K. Kremer, *Macromolecules* **21**(9), 2819 (1988).
 - ¹⁷ H. Hervet and C. P. Bean, *Biopolymers* **26**, 727 (1987).
 - ¹⁸ R. Azuma and H. Takayama, in *Computational Physics and Related Topics*, edited by Y. Hiwatari, Y. Oyanagi, Y. Okabe, and H. Takayama, The 5th International Conference on Computational Physics (Prog. Theor. Phys. Suppl., Kanazawa, Japan, 2000), 138, pp. 330–335.
 - ¹⁹ M. Matsumoto and M. Doi, *Molecular Simulation* **12**, 219 (1994).
 - ²⁰ R. Azuma and H. Takayama, preprint (2001).
 - ²¹ Y. Masubuchi, H. Oana, M. Matsumoto, and M. Doi, *Macromolecules* **30**, 912 (1997).

²² Y. Masubuchi, H. Oana, and M. Matsumoto, in *Computational Physics as a New Frontier in Condensed Matter Research*, edited by H. Takayama, M. Tsukada, H. Shiba, F. Yonezawa, M. Imada, and Y. Okabe (The Physical Society of Japan, Tokyo, Japan, 1995), pp. 347–354.

Figures

FIG. 1: The normalized histograms r_n and $r_{\Delta u}$ of a chain with $M = 160$ under $E = 0$ for various $k_B T$ obtained by the BD calculation.

FIG. 2: $\Omega_{\Delta u}$ versus $k_B T$.

FIG. 3: The mean peak shape $\bar{R}_l(t - t_{\max})/\bar{R}_l(t_{\max})$ of $M = 160$ with $a_{\text{gel}} = 20$ under $E = 0.032$. In each of the four intervals indicated by the arrow, histograms of $N_n(t)$ and $N_{\Delta u}(t)$ of a sequential 2000 steps are accumulated.

FIG. 4: Normalized histograms $r_n(t)$ represents characteristic instantaneous distributions of n for the intervals defined in Fig. 3.

FIG. 5: Normalized histograms $r_{\Delta u}(t)$ in the four intervals.

FIG. 6: r_n by the BD calculation.

FIG. 7: $r_{\Delta u}$ by the BD calculation.

FIG. 8: The normalized histograms r_n and $r_{\Delta u}$ under $\Theta = 0$ obtained by the EBFM.

FIG. 9: The normalized histogram $r_n(t)$ obtained by the EBFM.

FIG. 10: The normalized histogram $r_{\Delta u}(t)$ obtained by the EBFM.

FIG. 11: $r_{\Delta u}$ in the EBFM with various field strength Θ .

FIG. 1

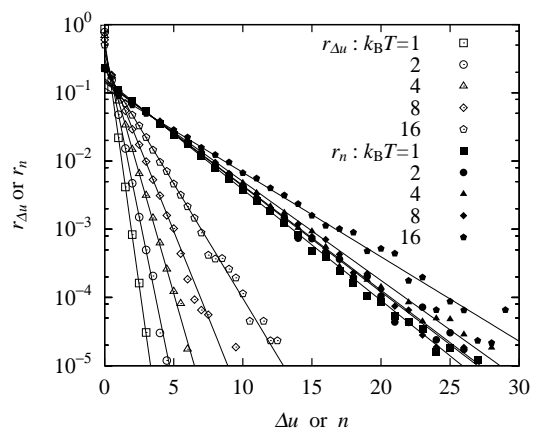


FIG. 2

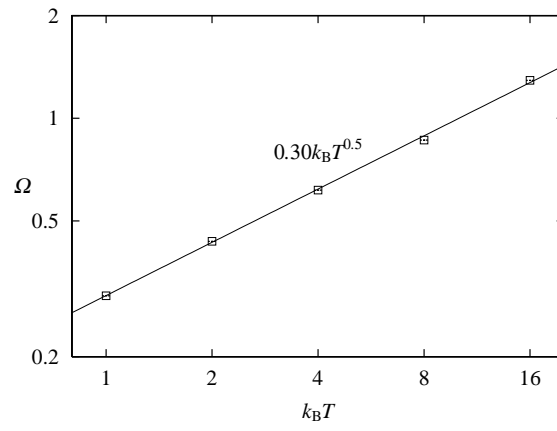


FIG. 3

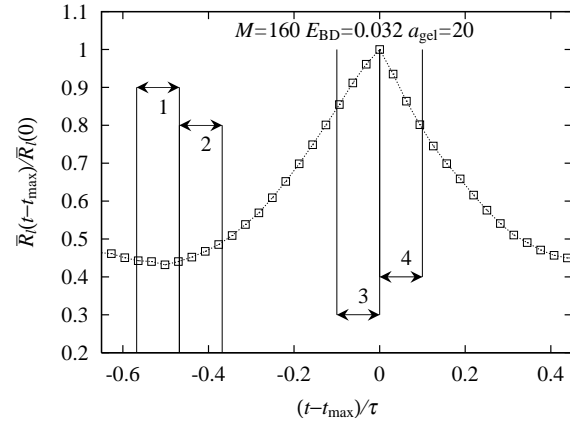


FIG. 4

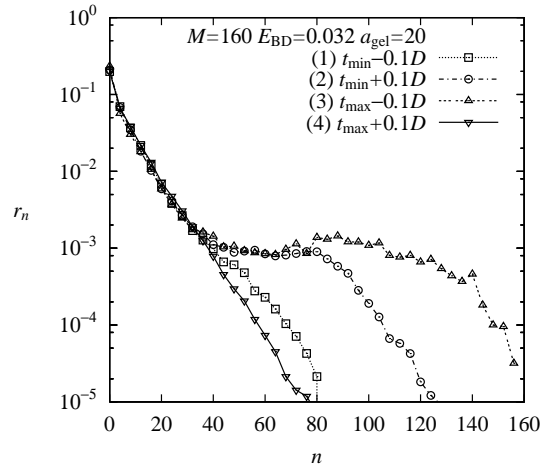


FIG. 5

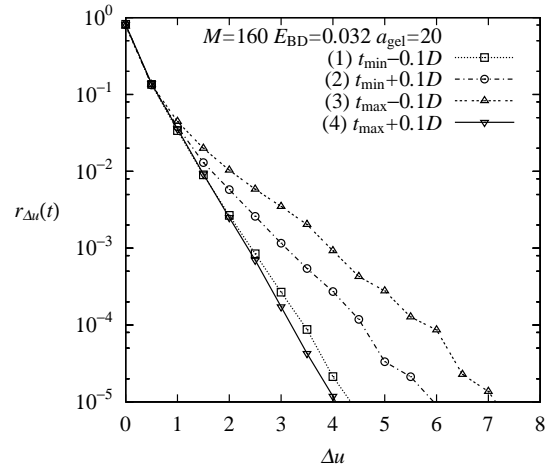


FIG. 6

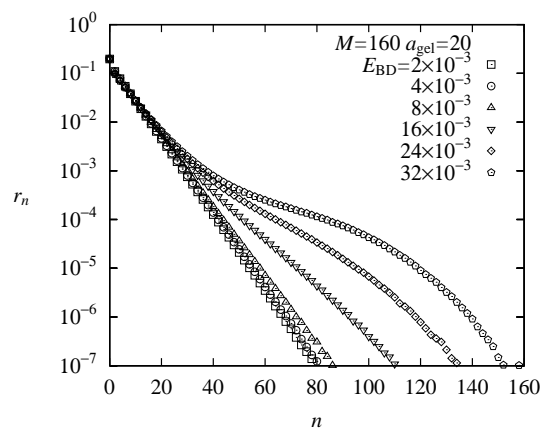


FIG. 7

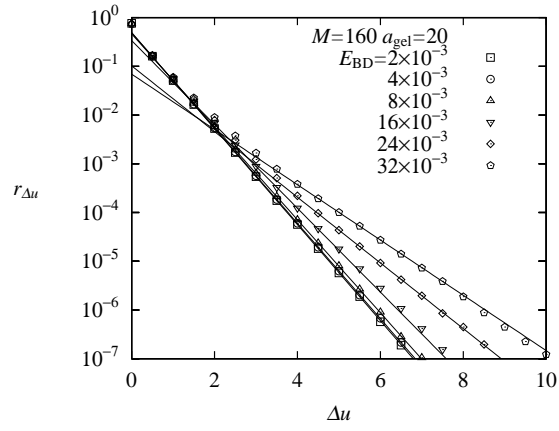


FIG. 8

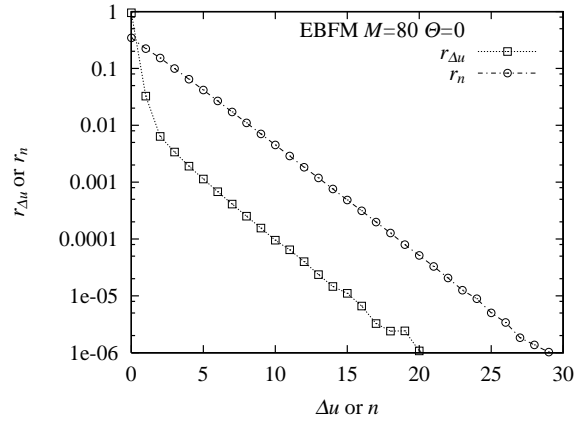


FIG. 9

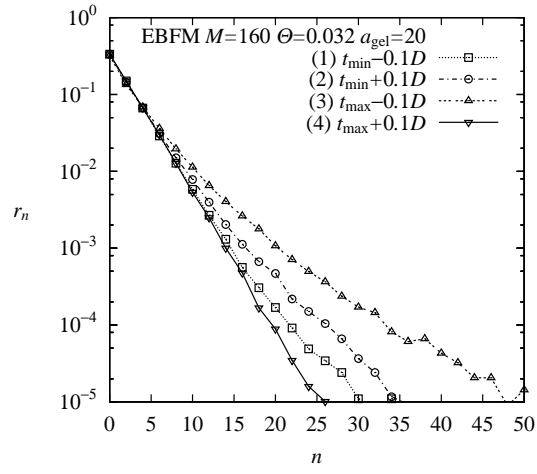


FIG. 10

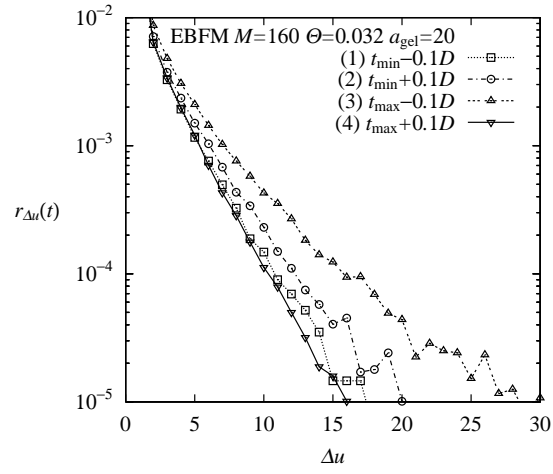


FIG. 11

